frontiers | Frontiers in Earth Science

ORIGINAL RESEARCH
published: 10 May 2022
doi: 10.3389/feart.2022.904932

Geochemical Characteristics and Fluid Properties of the Qixia Formation Dolomites of the Middle Permian in the Shuangyushi Block, NW Sichuan Basin, China

Wenli Xu[1,2], Gang Zhou[3]*, Cixuan Wan[4], Lianjin Zhang[5], Jiali Tao[3], Changhai Xu[3] and Xue Yan[6]*

[1]Institute of Sedimentary Geology, Chengdu University of Technology, Chengdu, China, [2]State Key Laboratory of Oil and Gas Reservoir Geology and Exploitation, Chengdu University of Technology, Chengdu, China, [3]Research Institute of Exploration and Development, PetroChina Southwest Oil and Gas Field Company, Chengdu, China, [4]Changqing Oilfield Company, Xi'an, China, [5]Central Sichuan Gas Field of Southwest Oil and Gas Field Company, PetroChina, Suining, China, [6]Sichuan Institute of Nuclear Industry Geology, Chengdu, China

OPEN ACCESS

Edited by:
Chen Zhang,
Chengdu University of Technology, China

Reviewed by:
Zhonggui Hu,
Sedimentology; Sequence Stratigraphy; Geochemical, China
Ziye Lu,
Southwest Petroleum University, China

***Correspondence:**
Wenli Xu
xuwenli5@163.com
Gang Zhou
zhougang29@126.com

Specialty section:
This article was submitted to Structural Geology and Tectonics, a section of the journal Frontiers in Earth Science

Received: 26 March 2022
Accepted: 20 April 2022
Published: 10 May 2022

Citation:
Xu W, Zhou G, Wan C, Zhang L, Tao J, Xu C and Yan X (2022) Geochemical Characteristics and Fluid Properties of the Qixia Formation Dolomites of the Middle Permian in the Shuangyushi Block, NW Sichuan Basin, China. Front. Earth Sci. 10:904932. doi: 10.3389/feart.2022.904932

On the basis of petrology, in combination with analysis of the geochemical characteristics of major and trace elements, REE (rare earth elements), carbon isotopes, oxygen isotopes, strontium isotopes and fluid inclusions, the geochemical characteristics and fluid properties of the Qixia Formation dolomites of the Middle Permian Qixiain the Shuangyushi block in the NW Sichuan Basin were systematically studied. The analysis results of the samples show that the Qixia dolomites are mainly composed of medium, coarse, medium-coarse crystalline and dolomites with polymodal crystal size distribution, and cloudy centers and clear rims. They generally show dark purple cathodoluminescence (CL) colors in the centers and orange red CL colors in the rims. The Qixia dolomites are relatively highly ordered (0.79–0.95, averaging 0.90). The CaO and MgO contents show a negative correlation. They are characterized by higher Mg/Ca ratio (0.89–0.92, averaging 0.91), high Fe (94–2,991 ppm, averaging 622 ppm), high Mn (26–185 ppm, averaging 102 ppm), high Na (210–374 ppm, averaging 277 ppm) contents, low Sr (53–218 ppm, averaging 93 ppm) content and lower ∑REE (1.10–5.56 ppm, averaging 2.08 ppm) concentrations. The REE patterns of the dolomites are similar to those of the calcites (C1), and are characterized by light REE (LREE) enrichment, heavy REE (HREE) depletion (LREE/HREE = 5.38–9.58, averaging 7.10), and Eu (0.65–4.19, averaging 1.70) and Ce (0.99–9.52, averaging 2.61) positive anomalies. They have consistent $\delta^{13}C$ (1.98–4.27‰ VPDB, averaging 3.01‰ VPDB) and $\delta^{18}O$ (–9.54‰––4.65‰ VPDB, averaging –7.09‰ VPDB) values with the coeval seawater. The salinity index Z is larger than 120, with diagenetic temperature higher than normal temperature. The average value of $^{87}Sr/^{86}Sr$ is positive (0.707150–0.712273, averaging 0.708669), while some samples are consistent to those of the coeval seawater. Their homogenization temperatures of fluid inclusions (96.3°C–105.0°C, averaging 101.1°C) exceed 100°C, which is equivalent to the buried paleogeothermal temperature, and their salinity (12.3%–14.3%, averaging 13.5%) is 3–5 times that of normal seawater. Based on the regional geological setting and

previous research achievements, the dolomitized fluids in the Qixia Formation are probably derived from seawater or marine fluids sealed in pores under shallow-burial environment. The dolomites experienced late alternation by deep high-salinity hydrothermal fluids, and were formed before the Middle-Late Triassic Period.

Keywords: dolomite, geochemical characteristics, Qixia formation, Shuangyushi block, analysis of fluid property

1 INTRODUCTION

The Shuangyushi block is located in the northwestern Sichuan Basin, covering an area of about 592.8 km^2. In recent years, significant breakthroughs in the oil and gas exploration of the Middle Permian Qixia dolomites have been achieved, and high-yield wells, such as Well SYX131 yielding 123.97×10^4 m^3 gas per day (Zeng et al., 2020). With the increasing exploration and development in this block, significant investigations on the genetic mechanism and fluid properties of dolomite reservoirs have been conducted, but a unified understanding has not been formed, which limited the follow-up exploration. The former research results indicated that the lenticular dolomites of the Qixia Formation in the western Sichuan Basin is originated by mixing water dolomitization (Zhang, 1982; Jiang et al., 2009), where Mg^{2+} is derived from seawater, magnesium-rich calcite red algae, sponges, bryozoans, echinoderms and other organisms (Zhang, 1982). The massive and patchy dolomites of the Qixia Formation in eastern Yunnan-western Sichuan are formed in the burial environment at higher temperatures, where Mg^{2+} is derived from the leaching of Emeishan basalt by meteoric water (Jin and Feng 1999). The Qixia Formation dolomites in northwestern Sichuan are formed by buried dolomitization (Jiang et al., 2009; Wang et al., 2011), where Mg^{2+} is mainly derived from clay mineral alteration, pressure dissolution of organic matter, magnesium-rich groundwater with incomplete metasomatism in its underlying strata and its overlying Emeishan basalt (Wang et al., 2011). The Qixia Formation dolomites in the northwestern Sichuan Basin are hydrothermal dolomites formed by the upwelling of deep fluids along faults (Huang et al., 2012, 2013; Yang et al., 2019). The Qixia Formation dolomites in the northwestern Sichuan Basin are regarded as the result of mixing water, burial and hydrothermal dolomitization (Tian et al., 2014). The Qixia Formation dolomites in the northwestern Sichuan Basin are formed by a superposition of buried dolomitization and later hydrothermal transformation, where Mg^{2+} mainly comes from seawater Meng et al., 2017; Hu et al., 2018; Zeng et al., 2020). No unanimous conclusion has been drawn on the genetic mechanism and fluid properties of the Qixia Formation dolomites in the northwestern Sichuan Basin. The increased data and deepened understanding are more and more supportive of the burial or hydrothermal dolomitization or their superimposition, the dolomitization fluids are derived from primary seawater, formation-sealed hot brine and deep hydrothermal solution etc. However, further research is needed into the specific formation mechanism and fluid properties of the Qixia Formation dolomites in the Shuangyushi block, northwestern Sichuan Basin. Therefore, this paper analyzed the petrological and geochemical characteristics of the Qixia Formation dolomites, and discussed the genetic mechanism and fluid properties on the basis of the analytical results, so as to provide support to the viewpoints on the dolomite genesis and provide guidance for further oil and gas exploration of the Qixia Formation dolomites in the Shuangyushi block, northwestern Sichuan Basin.

2 GEOLOGICAL BACKGROUNDS

Geotectonically, the Shuangyushi block is part of the northwestern margin of the Upper Yangtze Plate. It is located within the transition zone from the Longmenshan fault-fold belt to the low structural belt of the Central paleo-depression in the northern Sichuan Basin (Zeng et al., 2020), which borders the Longmenshan over-thrust belt to the west, the structural lowland in the Central paleo-depression in the northern Sichuan Basin to the east, and the piedmont fault-fold belt on the southern margin of the Micangshan Uplift to the north (**Figure 1**). The study area underwent two major structural evolution stages: the Sinian-Middle Triassic marine basin and the Meso-Cenozoic foreland basin (Chen et al., 2019). The Yunnan movement at the end of the Carboniferous Period caused a long-term weathering and denudation in the Sichuan Basin and its adjacent areas. In the Early Permian, a new marine transgression happened in the Sichuan Basin. Consequently, in the initial stage of transgression, the coal-bearing clastic rocks of the Lower Permian Liangshan Formation of shore-swamp facies were deposited above the Carboniferous weathering crust, with a thickness ranging from 0.2 to 30 m. With the expansion of transgression, the Qixia Formation carbonate sediments of the Middle Permian were developed within the basin (Huang et al., 2004). In general, the sea level rose first and then dropped. Affected by the ancient landform before the deposition of the Qixia Formation, the NW-SE extending basin-foreslope facies, platform margin facies and open platform facies were developed successively from northwest to southeast in the northwestern Sichuan Basin, and the Shuangyushi block was generally located in the platform margin facies belt (**Figure 1**), with a sediment thickness ranging from 70 to 300 m. During the early depositional stage of the Qixia Formation, the rapid rising of sea level led to a deep-water paleo-environment in the platform margin, allowing the formation of low-energy shoal sediments, which are mainly composed of dark gray medium- and thick-layer bioclastic wackestone or bioclastic packstone. During the middle-late deposition stages of the Qixia Formation, the platform-marginal low-energy shoal facies gradually evolved into the platform-marginal high-energy shoal facies, as the sea level inclined. The lithology was mainly light gray, gray-white thick-layer to massive sparry bioclastic grainstone and intraclastic

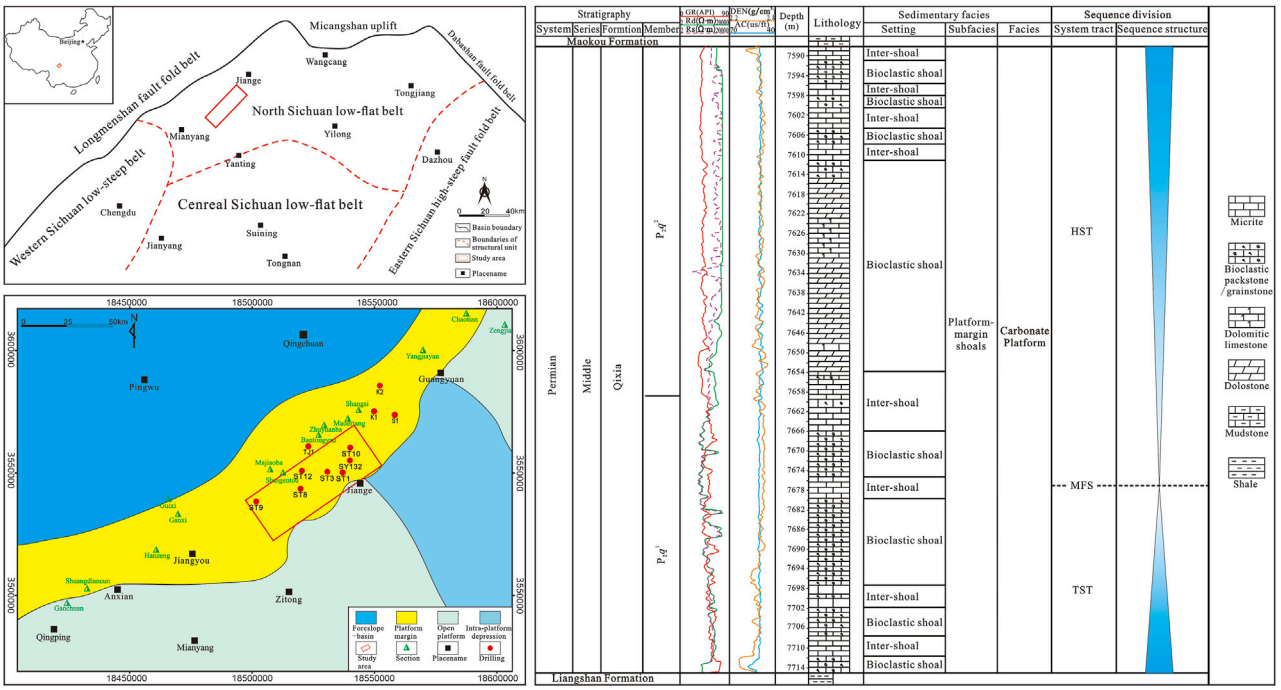

FIGURE 1 | Regional structure, sedimentary facies and comprehensive histogram of the Qixia Formation, Shuangyushi block.

TABLE 1 | Investigated samples of carbonates in the Qixia Formation.

Well no Number Type	Limestone	Dolostone	Limy dolostone	Dolomitic limestone	Dolomite	Calcite
ST2	12	0	0	0	0	0
ST3	10	73	0	0	1	0
ST8	6	57	2	2	1	0
MET	29	33	0	2	0	2
SGT	31	10	1	1	0	0

dolomite. In the late deposition stage of the Qixia Formation, the slight rise and fluctuation of sea level resulted in the gradual lithological variation into limy dolomite or dolomitic limestone, and bioclastic packstone intercalated with micrite. At the end of Qixia Formation, the large-scale rise of sea level occurred, leading to the regional deposition of thin mudstone or micrite at the bottom of the Maokou Formation, which covers the Qixia Formation with a conformable contact (Liu et al., 2021). The volcanic eruption in Emeishan area in the southwest during the sedimentary period of the Maokou Formation (Zhu et al., 2010) changed the thermal evolution history of the Sichuan Basin. Scholars reported that this igneous activity had a significant impact on the shallow buried Qixia Formation, and it made the Qixia Formation characterized with favorable source-reservoir configuration, larger trap closure, good preservation conditions and hydrocarbon accumulation in the Shuangyushi block, together with the later diagenesis and tectonism (Yang et al., 2018).

3 SAMPLES AND METHODS

Two hundreds and seventy-two samples were collected from the cores of the Qixia Formation (164) in the Shuangyushi block, Maoertang section (66) and Shuigentou section (43), including 88 limestone samples, 173 dolostone samples, 5 dolomitic limestone samples, 3 limy dolostone samples, 2 calcite samples and 2 dolomite samples (**Table 1**). They were prepared for thin section authentication, cathodoluminescence analysis, X-ray diffraction analysis, SEM observation, measurements of major elements, trace elements, carbon and oxygen isotopic compositions, strontium isotopes and fluid inclusions, which were completed in the State Key Laboratory of Oil and Gas Reservoir Geology and Exploration affiliated to Chengdu University of Technology.

The thin sections were identified and photographed by a Leica PM4500 optical microscope from Leica, Germany, after alizarin red staining. The cathodoluminescence analysis was conducted using a

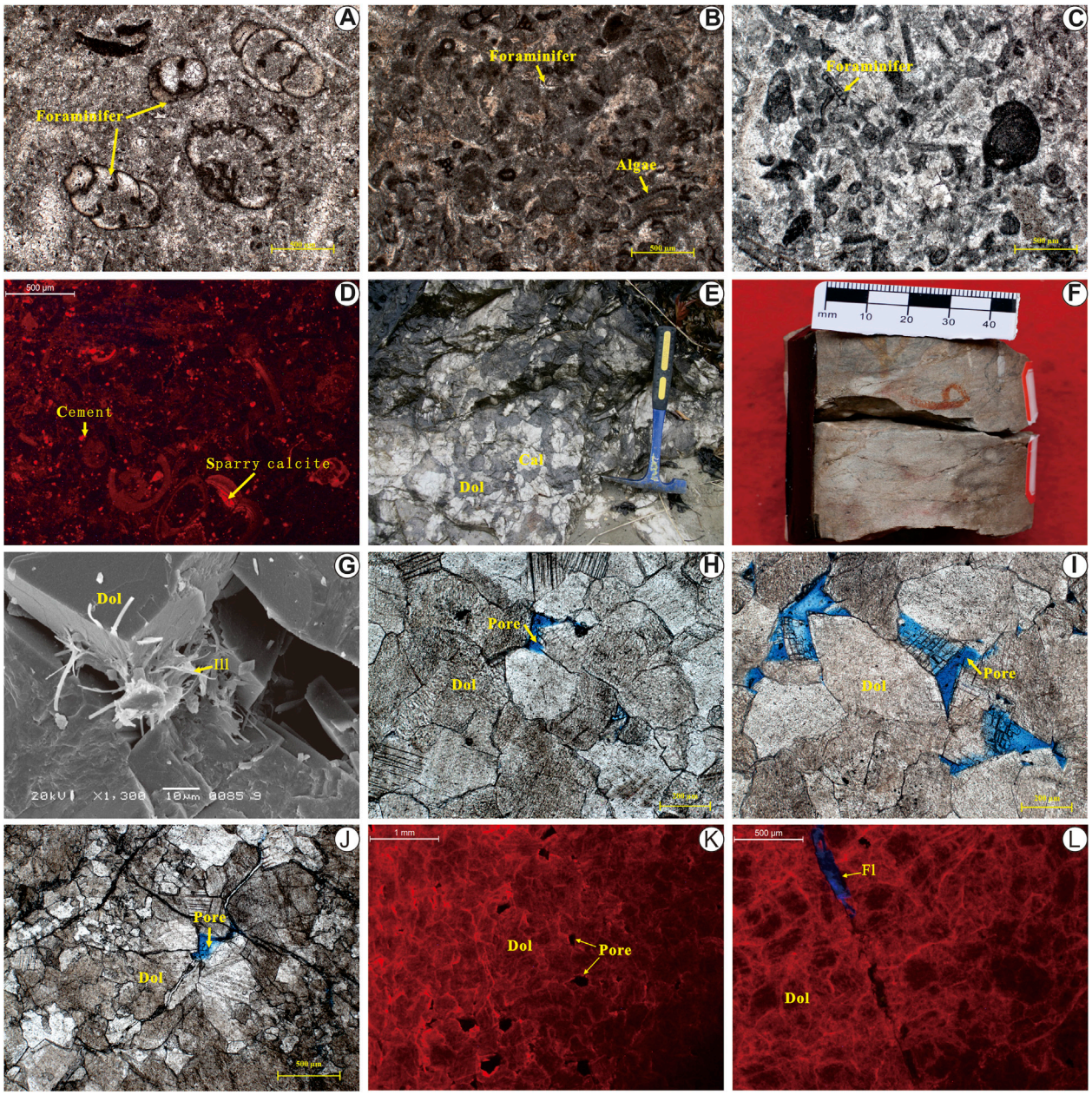

FIGURE 2 | Typical types of carbonates and their characteristics of the Qixia Formation:**(A)** Bioclastic wackstone, with foraminiferal fossils, 10 layers, Shuigentou section; **(B)** Bioclastic packstone, with algae and foraminifera fossils, 12 layers, Maoertang section; **(C)** Bioclastic grainstone, with foraminiferal fossils, 7,432.12 m, Well ST3; **(D)** Bioclastic packstone. The main part exhibits blue-violet luminescence and cements show orange red luminescence. Some bioclasts filled by sparry calcite display orange red luminescence, 5,739.41 m, Well ST2; **(E)** "Leopard" limestone, with leopard patches occurring in networks, 30 layers, Maoertang section; **(F)** Cracked dolomite, 7,328.93 m, Well ST8; **(G)** Dolomite with intergranular pores filled by hair-like illite, 7,326.95 m, Well ST8; **(H)** Mesocrystalline dolomite with intergranular pores, 7,323.85 m, Well ST8; **(I)** Coarse crystalline dolomite with intergranular pores; **(J)** Intergranular pores and fractures in dolomites with polymodal crystal size distribution, 7,330.90 m, Well ST8; **(K)** Zonal texture formed by dolomite crystals, dark purple luminescence in the centers and orange red luminescence in the rims, null in the pores, 7458 m, Well ST3; **(L)** Dolomite fractures filled with fluorite exhibiting indigo blue luminescence, 7,319.3 m, Well ST8.

CL8200 MK5–2 cathodoluminescence spectroscope from Cambridge Image Technology Ltd., United Kingdom, in conjunction with a Leica polarizing microscope, at the beam-focus voltage of 12 kV and the beam current of 300 μA. A D/MAX-IIIC diffractometer from Rigaku Company, Japan, was used for X-ray diffraction analysis. The SEM observation was performed using a JSM-5500LV SEM from JESOL Company, Japan and a QUANTAX400 X-ray energy spectrometer from Bruker Nano GmbH Company, Germany at the voltage of 20 kV and the current of 3×10^{-10} A. The major element measurement was conducted at the temperature of 20°C and humidity of 65%, using an ICP-OES from German SPECTRO Company. The trace element

measurement was performed at the temperature of 20°C and humidity of 65%, using an ICP-MS from Thermo Fisher Company, United States, at the temperature of 20°C and humidity of 65%. Carbon and oxygen isotopic compositions were obtained by an Elementar Isoflow-Precision from Elementar Company, German, according to the SY/T6039-94 and TTB-2 industrial standards, at the temperature of 20°C and humidity of 44%, with the analysis error of 0.01%. Measurement of Sr isotopic ratios was performed at the temperature of 20°C and humidity of 30% by using a MC-ICP-MS (Multi-Collector-Inductively Coupled Plasma Mass Spectrometry) from Thermo Fisher Company, United States, with the certified reference material NBS987 by NIST (National Institute of Standards and Technology) used as test standard. The error of the measured $^{87}Sr/^{86}Sr$ values ranges from 0.000010 to 0.000097, averaging 0.000043, which achieved the required accuracy for this study. The fluid inclusions were analyzed using a Linkam THMSG600 from Lincoln Company, United Kingdom.

The REE concentrations are normalized to those of the North American shale composite (NASC, Gromet et al., 1984) and anomalies of Cerium $(Ce/Ce^*)_{SN} = Ce_{SN}/(0.5La_{SN} + 0.5Pr_{SN})$, Europium $(Eu/Eu^*)_{SN} = Eu_{SN}/(0.67Sm_{SN} + 0.33Tb_{SN})$ were calculated based on the equations by Bau and Dulski (1996).

4 PETROGRAPHY

The Qixia Formation in the Shuangyushi block mainly consists of platform margin facies sediments, including limestone, dolomitic limestone, limy dolostone, dolostone and shale, with crystalline granular texture and grain texture observed.

4.1 Limestones

Limestones are widely developed in the study area, including micrite, bioclastic packstone and grainstone classified by texture.

Micrite is dominated by bioclastic wackstone (**Figure 2A**), and micrite is less developed or basically undeveloped. Macroscopically, it commonly occurs as gray-dark gray medium-thin layers, and also thick layers and masses. It is composed of microcrystalline calcite, where the bioclasts include foraminifera, crinoids, brachiopods, etc. According to its lithological association sequences, it was formed in the stable and low-energy environment between beaches.

Bioclastic packstone (**Figure 2B**) and grainstone (**Figure 2C**) are composed of calcites (C1), displaying a light gray, gray or brownish gray color, where the bioclasts include foraminifera, brachiopods, bryozoans, spines, bivalves, algae and etc., with a small amount of sand debris locally. The bioclastic packstone mainly cemented by microcrystalline calcite has relatively high shale content and is generally formed in the shoal margin. The bioclastic grainstone cemented by sparry calcite has relatively low shale content and is generally formed in the high-energy shoal core. The bioclastic packstone mainly shows blue-violet luminescence, and its calcite cements exhibit consistent luminescence with its surrounding rock. As replaced by calcite, the interior of some bioclasts displays orange red luminescence (**Figure 2D**).

The investigated carbonates are not completely dolomitized, which are predominantly composed of dolomitic limestones and a minor amount of limy dolostones. The lithology also known as "leopard" limestone, with fractures developed, which is easy to identify on the outcrops. The contact of dolomitic patches and limestone matrix is sharp, forming a clear boundary between them. Dolomitic patches are dark gray-gray black, and generally distributed in floating state within light gray, gray white limestone matrix. Locally, these patches are connected with each other, forming a network distribution (**Figure 2E**). They are mainly composed of fine-medium crystalline dolomite and mesocrystalline dolomite. Their crystals show better morphology and straight planar face, characterized with cloudy centers and clear rims (CCCR). Argillaceous materialis observed in dolomite locally. Limestone matrix is composed of bioclastic packstone with a high bioclastic content. The cements are mainly micritic calcite and some are sparry calcite. The bioclasts are dominated by ostracoda and echinoderms. According to the petrological features, it is generally formed in the shoal margin environment.

4.2 Dolostones

The Qixia Formation dolostones in the study area are mainly light gray-gray, thick-massive crystalline dolomites (D1) formed by recrystallization, with pores and fractures developed. Fractures are completely or incompletely filled with crystallized calcites (C2), saddle dolomites (D2), asphalt and clay minerals (**Figure 2F**) and a small amount of fluorite, apatite and other hydrothermal minerals. Pores are completely or incompletely filled with anhedral dolomites (D3). Locally, the crystalline dolomites are cut into brecciated dolomite or cataclastic dolomite by fractures (**Figure 2G**). The dolomites are highly crystallized, and mainly consist of medium crystals (**Figure 2H**), coarse crystals (**Figure 2I**), medium-coarse crystals and anisotropic crystals (**Figure 2J**), which are mainly euhedral and semi-euhedral with straight crystal face, and anhedral with non-straight crystal face. The crystals are turbid. The original texture of the dolomites has completely disappeared, and the ghosts of bioclasts, including foraminifera, spines and etc. were observed locally. Thus, the original rock was inferred as bioclastic limestone, which was formed in the high-energy shoal core. In the cathodoluminescence (CL) images, zonation of the dolomite crystals was observed. The cores exhibit dark purple luminescent (**Figure 2K**), representing the early growing dolomites, and the rims generally show bright orange red luminescent (**Figure 2K**), representing the late growing dolomites. The fluorite and dolomite filling fractures display indigo blue luminescent (**Figure 2L**) and dark purple luminescent, respectively.

4.3 Shales

Little amount of shales are developed in the study area. They are generally gray and gray black, with smaller thickness, mainly formed in the low-energy inter-beach environment.

5 RESULTS

5.1 XRD

QixiaX-ray diffraction data are given in **Table 2**. The order degree of dolomite (D1) varies from 0.79 to 0.95, averaging 0.90.

TABLE 2 | XRD composition of dolomites in the Qixia Formation.

Sample no	Depth(m)	Description	Degree of order
ST3-56	7,449.09	D1	0.91
ST3-60	7,449.44	D1	0.94
ST3-78	7,458.00	D1	0.89
ST3-87	7,460.40	D1	0.79
ST8-90	7,319.30	D1	0.95
ST8-102	7,323.70	D1	0.93
ST8-114	7,326.95	D1	0.87
ST8-123	7,328.38	D1	0.92
ST8-16	7,330.90	D1	0.92

5.2 Geochemistry

5.2.1 Major and Trace Elements

Major and trace elements data are given in **Table 3**. C1 have high CaO content (51.1%–52.8%, averaging 52.3%), and low MgO content (0.7%–1.9%, averaging 1.3%). D1 have relatively high CaO content (28.7%–30.4%, averaging 29.7%) and slightly low MgO (19.6%–20.4%, averaging 20.0%). The Mg/Ca ratio ranges from 0.89 to 0.92, averaging 0.91.

In C1, the Fe content ranges from 29 to 1,253 ppm, averaging 291 ppm; the Mn content from 9 to 70 ppm, averaging 44 ppm; and the Sr content from 82 to 2,221 ppm, averaging 630 ppm. In D1, the Fe content varies from 94 to 2,991 ppm, averaging 622 ppm; the Mn content from 26 to 185 ppm, averaging 102 ppm; and the Sr content from 53 to 218 ppm, averaging 93 ppm. In D2, the Fe, Mn and Sr contents are 25 ppm, 269 and 94 ppm, respectively. In C2, the Fe, Mn and Sr contents are 17 ppm, 73 and 141 ppm, respectively. The Na content in C1 ranges between 94 and 260 ppm, averaging 157 ppm, and that in D1 ranges between 210 and 374 ppm, averaging 277 ppm.

Rare earth element (REE) data are given in **Table 4**. The average ΣREE, LREE/HREE ratio, $(Ce/Ce^*)_{SN}$ and $(Eu/Eu^*)_{SN}$ value of C1 is 3.44 ppm (1.04–10.50 ppm), 9.95 (5.44–20.5), 0.84 (0.40–1.36) and 1.01 (0.60–1.37), respectively. The average ΣREE, LREE/HREE ratio, and $(Ce/Ce^*)_{SN}$ value of D1 is 2.08 ppm (1.10–5.56 ppm), 7.10 (5.38–9.58), and 0.96 (0.64–1.54), respectively. The $(Eu/Eu^*)_{SN}$ value varies from 0.65 to 4.19, averaging 1.70, when an extremely high value of 24.29 is excluded. The ΣREE, LREE/HREE ratio, $(Ce/Ce^*)_{SN}$ and $(Eu/Eu^*)_{SN}$ value of D2 is 1.85 ppm, 11.33, 0.74 and 0.95, respectively. The ΣREE, LREE/HREE ratio, $(Ce/Ce^*)_{SN}$ and $(Eu/Eu^*)_{SN}$ value of C2 is 3.93 ppm, 12.24, 0.93 and 0.43, respectively.

5.2.2 Isotopic Values

Carbon and oxygen isotopic data are given in **Table 5**. The $\delta^{13}C$ and $\delta^{18}O$ of C1 are −1.02‰–3.16‰ VPDB (averaging 1.77‰ VPDB) and -8.13‰ to -6.18‰ VPDB (averaging -7.16‰ VPDB), respectively. The $\delta^{13}C$ and $\delta^{18}O$ of D1 are 1.98‰–4.27‰ VPDB (averaging 3.01‰ VPDB) and −9.54‰ to −4.65‰ VPDB (averaging −7.09‰ VPDB), respectively. The $\delta^{13}C$ and $\delta^{18}O$ of D2 are 2.58‰ and −11.21‰ VPDB. The $\delta^{13}C$ and $\delta^{18}O$ of C2 are 1.27‰–2.62‰ VPDB (averaging 1.95‰ VPDB) and −7.74‰ to −15.66‰ VPDB (averaging −11.7‰ VPDB).

Strontium isotopic data are given in **Table 5**. The $^{87}Sr/^{86}Sr$ ratio of C1 ranges from 0.707186 to 0.708478, averaging 0.707578; that of D1 varies between 0.707150 and 0.712273, averaging 0.708669; that of D2 is 0.708459; and that of C2 is 0.708422–0.708769, averaging 0.708596.

TABLE 3 | Major and trace elements of carbonates in the Qixia Formation.

Sample no	Depth(m)	Description	Major element (%)		Trace element (ppm)			
			CaO	MgO	Fe	Mn	Sr	Na
ST2-19	5,744.60	C1	51.1	1.5	197	50	1972	260
ST3-25	7,432.12	C1	52.8	0.7	1,253	50	231	202
ST8-22	7,322.50	C1	52.2	1.9	569	50	136	118
ST8-11	7,324.40	C1	—	—	234	9	273	—
MET-9	9.00	C1	—	—	84	70	167	—
MET-13	12.00	C1	—	—	57	39	504	—
MET-17	15.00	C1	—	—	29	30	2,221	—
MET-31	26.00	C1	52.7	1.3	100	50	82	111
MET-34	26.00	C1	52.7	1.2	100	50	85	94
ST3-34	7,448.20	D1	—	—	2,991	26	115	—
ST3-56	7,449.09	D1	28.7	19.6	230	131	113	374
ST3-60	7,449.44	D1	—	—	1877	35	98	—
ST3-78	7,458.00	D1	29.4	19.6	164	133	70	325
ST3-87	7,460.40	D1	30.1	20.0	665	139	74	249
ST8-90	7,319.30	D1	30.4	20.2	94	96	92	244
ST8-94	7,323.30	D1	29.2	20.0	173	147	71	210
ST8-102	7,323.70	D1	29.6	19.8	263	56	59	308
ST8-114	7,326.95	D1	30.4	20.1	305	185	218	328
ST8-123	7,328.38	D1	29.4	19.9	165	111	85	220
ST8-24	7,330.30	D1	30.1	20.4	224	113	63	236
ST8-16	7,330.90	D1	—	—	316	57	53	—
ST8-27	7,330.60	D2	—	—	25	269	94	—
MET-28	25.00	C2	—	—	17	73	141	—
ST2-19	5,744.60	C1	51.1	1.5	197	50	1972	260
ST3-25	7,432.12	C1	52.8	0.7	1,253	50	231	202

TABLE 4 | REE of carbonates in the Qixia Formation.

Sample no	Depth(m)	Description	La (ppm)	Ce (ppm)	Pr (ppm)	Nd (ppm)	Sm (ppm)	Eu (ppm)	Gd (ppm)	Tb (ppm)	Dy (ppm)	Ho(ppm)	Er (ppm)	Tm (ppm)	Yb(ppm)	Lu (ppm)	∑REE (ppm)	LREE/ HREE	$(Eu/Eu^*)_{SN}$	$(Ce/Ce^*)_{SN}$
ST2-19	5,744.60	C1	0.758	1.547	0.131	0.751	0.155	0.036	0.158	0.025	0.158	0.037	0.105	0.015	0.108	0.015	4.00	5.44	1.04	1.05
ST3-7	7,112.00	C1	2.898	2.449	0.623	2.274	0.541	0.138	0.535	0.075	0.410	0.093	0.227	0.031	0.185	0.024	10.50	5.65	1.20	0.40
ST3-25	7,432.12	C1	0.684	1.554	0.188	0.503	0.098	0.019	0.089	0.013	0.089	0.022	0.074	0.013	0.093	0.013	3.45	7.50	0.92	0.94
ST8-22	7,322.50	C1	0.215	1.034	0.111	0.406	0.087	0.024	0.091	0.010	0.081	0.020	0.051	0.007	0.049	0.005	2.19	5.98	1.37	1.36
ST8-11	7,324.40	C1	0.332	0.649	0.062	0.218	0.049	0.012	0.051	0.005	0.030	0.005	0.037	0.005	0.028	0.005	1.49	7.96	1.26	0.98
MET-31	26.00	C1	0.143	0.506	0.143	0.157	0.027	0.003	0.024	0.001	0.014	0.002	0.009	0.000	0.009	0.000	1.04	16.59	0.68	0.61
MET-34	26.00	C1	0.572	0.527	0.072	0.116	0.023	0.002	0.021	0.000	0.014	0.002	0.014	0.001	0.011	0.001	1.38	20.50	0.60	0.53
ST3-34	7,448.20	D1	0.650	1.206	0.121	0.357	0.101	0.023	0.068	0.013	0.091	0.022	0.066	0.009	0.049	0.009	2.79	7.52	1.10	0.93
ST3-56	7,449.09	D1	0.405	0.740	0.114	0.334	0.097	0.437	0.070	0.008	0.054	0.013	0.032	0.007	0.035	0.003	2.35	9.58	24.29	0.75
ST3-60	7,449.44	D1	0.482	0.878	0.094	0.398	0.080	0.012	0.070	0.014	0.061	0.017	0.050	0.005	0.043	0.005	2.21	7.34	0.65	0.89
ST3-78	7,458.00	D1	0.052	0.505	0.058	0.234	0.049	0.040	0.046	0.005	0.044	0.009	0.026	0.002	0.023	0.003	1.10	5.94	4.19	1.54
ST3-87	7,460.40	D1	0.354	0.530	0.075	0.307	0.065	0.030	0.071	0.008	0.062	0.013	0.036	0.005	0.032	0.004	1.59	5.89	2.25	0.71
ST8-90	7,319.30	D1	1.008	1.857	0.319	1.167	0.266	0.071	0.266	0.039	0.222	0.048	0.133	0.018	0.128	0.018	5.56	5.38	1.23	0.71
ST8-94	7,323.30	D1	0.237	0.427	0.074	0.272	0.054	0.030	0.058	0.005	0.040	0.008	0.031	0.002	0.022	0.004	1.26	6.44	2.92	0.70
ST8-102	7,323.70	D1	0.397	0.398	0.036	0.215	0.045	0.013	0.044	0.005	0.038	0.007	0.023	0.002	0.027	0.002	1.25	7.46	1.45	0.64
ST8-114	7,326.95	D1	0.303	0.780	0.090	0.307	0.066	0.021	0.074	0.008	0.063	0.013	0.044	0.006	0.033	0.003	1.81	6.42	1.56	1.02
ST8-123	7,328.38	D1	0.283	0.741	0.038	0.401	0.077	0.024	0.065	0.009	0.047	0.010	0.030	0.004	0.027	0.002	1.76	8.06	1.54	1.49
ST8-24	7,330.30	D1	0.314	0.682	0.056	0.330	0.075	0.013	0.060	0.008	0.053	0.011	0.031	0.004	0.030	0.004	1.67	7.31	0.88	1.11
ST8-16	7,330.90	D1	0.333	0.699	0.071	0.255	0.047	0.009	0.054	0.005	0.036	0.014	0.032	0.005	0.029	0.005	1.59	7.86	0.97	0.99
ST8-27	7,330.60	D2	0.514	0.741	0.089	0.315	0.034	0.007	0.051	0.005	0.039	0.008	0.023	0.005	0.014	0.005	1.85	11.33	0.95	0.74
MET-28	25.00	C2	0.968	1.770	0.174	0.631	0.085	0.008	0.129	0.013	0.068	0.014	0.032	0.005	0.031	0.005	3.93	12.24	0.43	0.93

TABLE 5 | Carbon, oxygen and strontium isotope of carbonates in the Qixia Formation.

Sample no	Depth(m)	Description	$^{87}Sr/^{86}Sr$	$\delta^{13}C‰$(VPDB)	$\delta^{18}O‰$(VPDB)
ST2-19	5,744.60	C1	0.707351	3.05	−6.59
ST3-7	7,112.00	C1	0.707186	—	—
ST3-25	7,432.12	C1	0.707320	—	—
ST8-22	7,322.50	C1	0.707499	−1.02	−6.96
MET-9	9.00	C1	0.707531	0.89	−6.18
MET-13	12.00	C1	0.707511	2.78	−8.13
MET-17	15.00	C1	0.708478	3.16	−7.96
MET-34	26.00	C1	0.707744	—	—
ST3-34	7,448.20	D1	0.707428	2.14	−6.23
ST3-56	7,449.09	D1	0.709255	4.27	−7.37
ST3-60	7,449.44	D1	0.707609	3.05	−4.65
ST3-78	7,458.00	D1	0.707997	3.36	−7.66
ST3-87	7,460.40	D1	0.708632	3.92	−6.62
ST8-90	7,319.30	D1	0.707487	2.88	−8.17
ST8-99	7,323.30	D1	0.707150	—	—
ST8-102	7,323.70	D1	0.708565	2.81	−6.37
ST8-114	7,326.95	D1	0.712273	1.98	−7.69
ST8-123	7,328.38	D1	0.711389	2.49	−6.55
ST8-24	7,330.30	D1	0.708256	—	—
ST8-16	7,330.90	D1	0.707984	3.16	−9.54
ST8-27	7,330.60	D2	0.708459	2.58	−11.21
MET-28	25.00	C2	0.708769	2.62	−15.66
MET-31	26.00	C2	0.708422	1.27	−7.74

TABLE 6 | The fluid inclusions homogenization temperature and salinity of carbonatesin the Qixia Formation.

Sample no	Depth(m)	Host mineral	Th (°C)	Salinity (%)
ST8-102	7,323.70	D1	96.9	12.8
			96.3	12.3
ST3-78	7,458.00	D1	102.5	13.8
			102.0	13.8
			105.0	14.3
			104.0	14.1
ST3-56	7,449.09	D2	129.7	22.0
			129.0	21.7
			128.5	21.4
			123.5	21.5
ST8-90	7,319.30	D3	114.3	21.3
			114.0	21.6
			115.0	21.9

5.3 Fluid Inclusion

Fluid inclusion data are given in **Table 6**. The homogenization temperature and salinity of inclusions in D1 are 96.3°C–105.0°C (averaging 101.1°C) and 12.3%–14.3% (averaging 13.5%), respectively. The homogenization temperature and salinity of inclusions in D2 are 123.5°C–129.7°C (averaging 127.7°C) and 21.4%–22% (averaging 21.7%), respectively. The homogenization temperature and salinity of inclusions in D3 are 114.3°C–115°C (averaging 114.4°C) and 21.3%–21.9% (averaging 21.6%).

6 INTERPRETATION AND DISCUSSIONS

6.1 Dolomite Petrography

The petrological characteristics show the Qixia Formation in the Shuangyushi block is dominated by medium crystalline, coarse crystalline, medium-coarse crystalline and dolomites with polymodal crystal size distribution characterized by coarse crystals with cloudy centers and clear rims. Their original rocks are mainly the bioclastic grainstones deposited in a high-energy shoal environment of platform margin, without gypsolyte or gypsum cements, salt rock and dolomicrite normally formed in an evaporitic environment or mode. The analyses by X-ray diffraction determined a high order degree of D1. This means that a dolomitization process characterized with relatively slower crystallization and higher crystallization degree, or a higher dolomitization temperature and relatively complete dolomitization are required to form the specific alternating arrangement of $CaCO_3$ and $MgCO_3$ layers under ideal conditions, leading to the higher order degree (Zhong et al., 2009). These characteristics indicate a metasomatic origin of the D1 under burial conditions without syngenetic dolomitization and mixing water dolomitization. The microscopically undulatory extinction observed in some dolomites suggests the influence of hydrothermal fluids in the burial process.

6.2 Major and Trace Elements

Among the major elements, CaO and MgO contents reflect the crystalline form of dolomites in some extent (Sun et al., 2018). In the dolomites of sedimentary genesis, Mg^{2+} and Ca^{2+} are precipitated as $CaMg(CO_3)_2$ by the ratio of 1:1. Both of the CaO and MgO contents increase with the increased amount of dolomites, showing a positive correlation. In the dolomites of metasomatic genesis, CaO content decreases and MgO content increases with the increase of metasomatic dolomites, showing a negative correlation (He et al., 2018). QixiaCaO and MgO contents have a negative correlation with each other of D1 (**Figure 3**), and Mg to Ca ratio is close to the stoichiometric value of ideal dolomites, which indicates a metasomatic genesis.

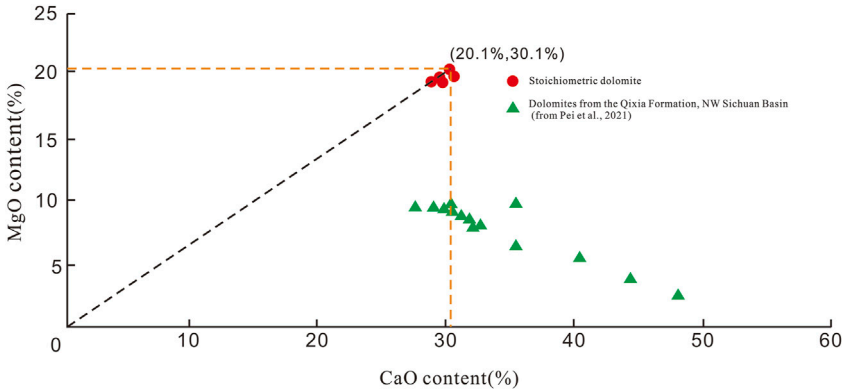

FIGURE 3 | Plot of CaO and MgO contents for the carbonates in the Qixia Formation.

Some trace elements (Na, Sr, Fe and Mn etc.) are important indicators of the sedimentary-diagenetic environment and the diagenetic fluid properties of rocks, which are effective in analyzing the origin of dolomites (Walker et al., 1989; He et al., 2018). Researches have proven the seawater is rich in Na, Sr and deficient in Fe, Mn; Fe, Mn contents increase and Sr content decreases with the enhanced diagenesis of marine carbonates because Na, Sr are brought out, while Fe, Mn are brought in as the overall trend of element migration in the diagenetic process (Ren et al., 2016; He et al., 2018), and Na is also controlled by the salinity of diagenetic fluids (Walker et al., 1989; He et al., 2014). The D1 of the Qixia Formation has low Sr content, higher contents of Fe, Mn and Na than the coeval marine limestone, which indicates the D1 are probably formed in the high-salinity environment under burial condition.

6.3 Rare Earth Elements

The distribution pattern of rare-earth elements (REE) is an indicator to identify the material source and is used to characterize the properties of dolomitization fluids. Ce^{3+} and Eu^{3+} are easy to form soluble ions with the change of physicochemical conditions and then separated from REE, leading to anomalies, which are used for determination of the diagenetic environment. QixiaThe ΣREE of C1 and C2 are within the variation range of normal marine carbonates of 1–50 ppm and are similar to each other. The ΣREE of D1 and D2 are lower than that of C1, indicating that the D1 and D2 retain the REE characteristics of their original calcites. The NASC-normalized REE patterns of C1, C2, D1 and D2 are similar to each other (**Figure 4**). The C1 show enrichment of LREE and depletion of HREE, and $(Eu/Eu^*)_{SN}$ values presenting slightly positive anomalies, with part of the values dominantly presenting negative anomalies, and $(Ce/Ce^*)_{SN}$ values presenting negative anomalies, with individuals presenting slightly positive anomalies. The D1 show enrichment of LREE and depletion of HREE, and $(Eu/Eu^*)_{SN}$ values presenting obviously positive anomalies, with individuals presenting slightly negative anomalies, and $(Ce/Ce^*)_{SN}$ values presenting slightly negative anomalies, with part of the values dominantly presenting positive anomalies. The D2 show enrichment of light REE and depletion of heavy REE, and $(Eu/Eu^*)_{SN}$ value showing a slightly negative anomaly, and $(Ce/Ce^*)_{SN}$ value presenting a negative anomaly. The C2 show enrichment of LREE and depletion of HREE, and $(Eu/Eu^*)_{SN}$ values presenting a negative anomaly, and $(Ce/Ce^*)_{SN}$ presenting a slightly negative anomaly.

The REE distribution pattern of D1 is similar to that of C1, which is characterized by enriched LREE, depleted HREE, obvious positive Eu anomalies, and slightly negative Ce anomalies. Eu is very sensitive to temperature. When a weak reducing environment is heated to above 250°C under increased pressure, Eu in fluid is easy to enter the lattices of hydrothermal minerals in the form of Eu^{2+}, forming strong positive anomalies. At the intermediate temperature of about 100°C, both Eu^{2+} and Eu^{3+} exist in fluid. In the low-temperature surface environment, Eu in fluid mainly appears in the form of Eu^{3+}. It tends to combine with oxygen and form oxide precipitation rather than entering the lattices of minerals, resulting in negative Eu anomalies in carbonate minerals (Li et al., 2021). Michard and Albarede, (1986) identified the characteristic high LREE enrichment and obvious Eu positive anomalies resulted from the reaction between seawater and ocean floor rocks at 350°C through a study on the high-temperature hydrothermal fluids in floor highs of the eastern Pacific Ocean. Yi et al. (2008) studied the Oligocene-Miocene lacustrine dolomites alternated by hydrothermal fluids in central Tibetan Plateau. Han et al. (2009) studied the Early Paleozoic hydrothermal dolomites in the Tarim Basin. Yang et al. (2014) studied the Shahejie Formation hydrothermal dolomites of the Paleogene in the Qikou sag. All these hydrothermal dolomites are characterized by high LREE enrichment and obvious Eu positive anomalies. Although some marine carbonates affected by hydrothermal fluids show depletion in LREE, they generally have obvious positive Eu anomalies. Ce anomaly generally refers to the enrichment degree of Ce relative to La and Pr. Under the oxygen-rich conditions, Ce^{3+} is partially oxidized into Ce^{4+} and precipitated adhering to the surface of manganese oxide (or hydroxide), leading to the negative anomalies of Ce due to the consequent consumption of Ce in seawater. The fractionation of Ce only occurs in an oxygen-rich environment, thus the Ce anomaly in marine sediments is applied as a sensitive paleoredox indicator. Based on the above-described principles and research results, dolomitization fluids in the Qixia Formation should be dominated by marine fluids. The Qixia Formation was influenced by high-salinity hydrothermal fluids in its burial process. As the un-dolomitized limestones were also

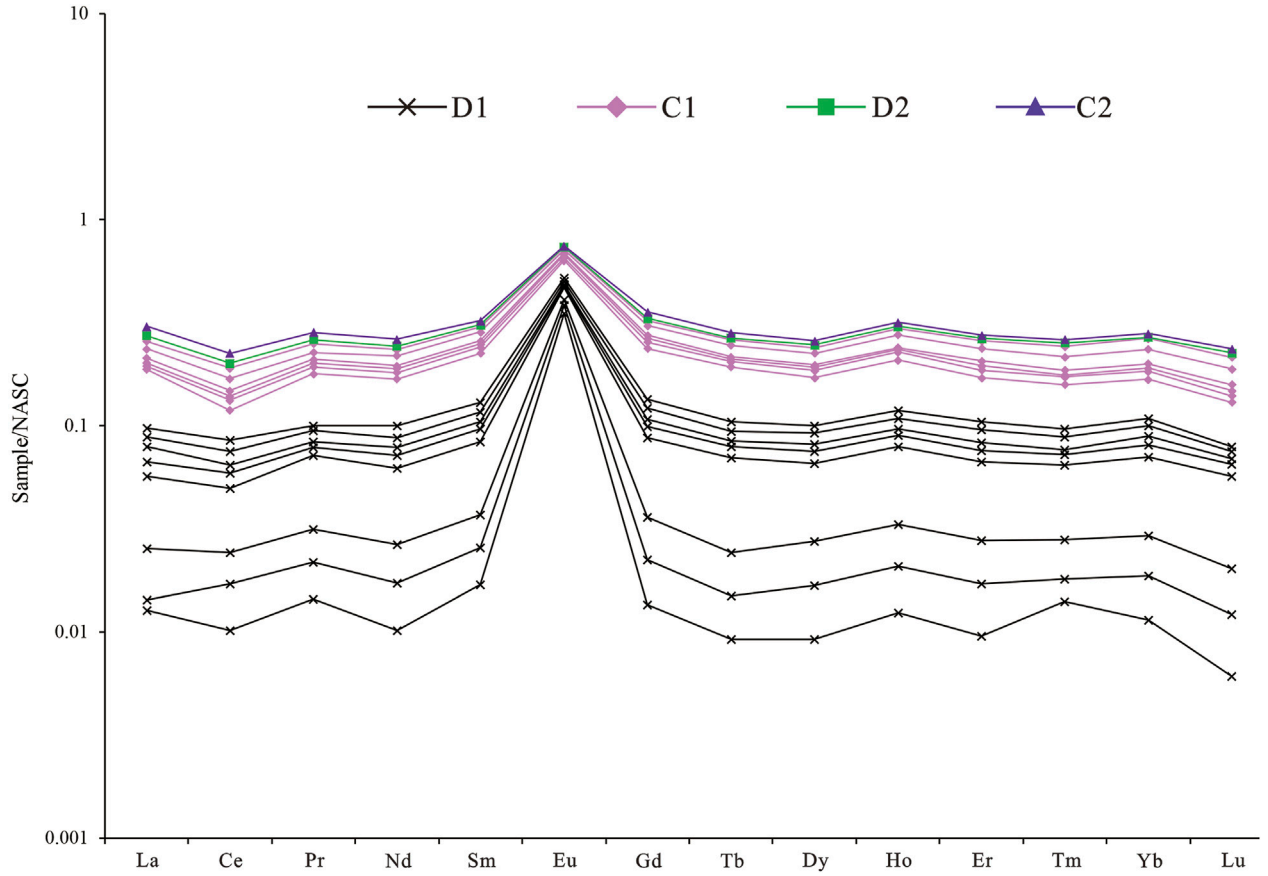

FIGURE 4 | REE distribution curves for the carbonates in the Qixia Formation.

affected by the fluids locally, resulting in the positive anomalies of Eu in some samples.

6.4 Carbon and Oxygen Isotopes

Carbon and Qixia oxygen isotope compositions are effective reflectors of the paleo-salinity and paleotemperature of rock formation, thereby they are used to determine the source of dolomitization fluids and the origin of dolomites (Jin et al., 2019). According to the studies on the Permian marine brachiopod fossils conducted by Veizer et al. (1999) and Jiang et al. (2016), the variation ranges of $\delta^{13}C$ and $\delta^{18}O$ have been determined as 0–4.8‰ VPDB and −10.0‰ to −5.0‰ VPDB respectively (**Figure 5**). It is concluded that the $\delta^{13}C$ and $\delta^{18}O$ of C1 and D1 in the Qixia Formation range within their variation ranges of the coeval seawater, and the $\delta^{18}O$ values of C2 and D2 are generally more negative than those of the coeval seawater, and the $\delta^{13}C$ values are within their variation range of the coeval seawater. According to Jiang et al. (2014), the $\delta^{13}C$ values of the Middle Permian medium-coarse crystalline dolomites in the western Sichuan Basin, ranging from 1.87‰ to 5.3‰ VPDB, showing small difference from those of the coeval seawater. As measured by Meng et al. (2017), the $\delta^{13}C$ values of the medium-coarse crystalline dolomites from the Qixia Formation of the Middle Permian in the western Sichuan Basin have an average value of

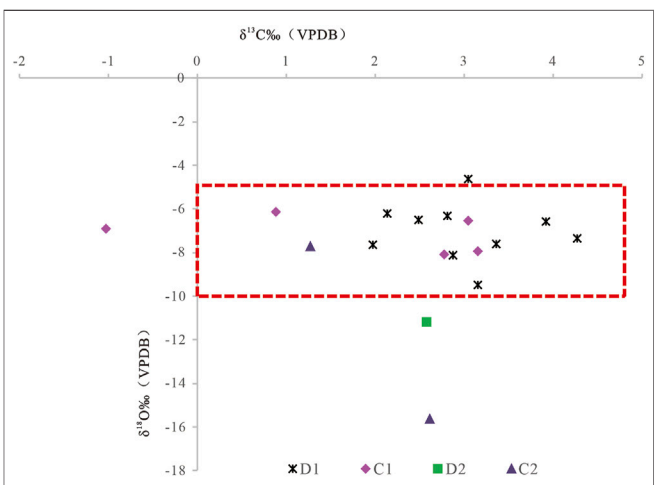

FIGURE 5 | Plot of $\delta^{13}C$ and $\delta^{18}O$ isotope for the carbonates in the Qixia Formation.

2.68‰ VPDB, and vary within the variation range of the coeval seawater. The results are similar to those measured in previous studies. It is indicated that the dolomitization fluids in the Qixia

Formation is mainly derived from the seawater or marine fluids in formation, and is affected by high-temperature hydrothermal solution.

6.5 Strontium Isotopic Composition

The strontium isotopic composition is an indicator of the source of dolomitization fluids (He et al., 2014). The $^{87}Sr/^{86}Sr$ values in the Middle-Lower Permian paleo-seawater were measured as 0.70613–0.70821 (Huang, 1997). The C1 shows a consistent variation range of $^{87}Sr/^{86}Sr$ with the coeval seawater, and the D1, C2 and D2 have higher $^{87}Sr/^{86}Sr$ values than the coeval seawater. The D1 has the highest average $^{87}Sr/^{86}Sr$, but the $^{87}Sr/^{86}Sr$ values of some D1 and C2 are lower than that of the coeval seawater.

Chen et al. (2013) reported that the $^{87}Sr/^{86}Sr$ ratio (0.709174–0.710194) of the Middle Permian hydrothermal dolomites is greater than that of the coeval marine limestones. Jiang et al. (2014), Meng et al. (2017) and Pei et al. (2021) reported the $^{87}Sr/^{86}Sr$ ratio varies within the variation range of the coeval seawater, which are similar to those measured in previous studies. Exceptionally in some dolomite samples, the $^{87}Sr/^{86}Sr$ values were measured higher than that of the coeval seawater. It is well known that the marine strontium isotopic composition in the geological history is a function of time, and the major controls over its variations are two sources of strontium. One is the chemical weathering of the continental old silicate rocks, which provides the radiogenic ^{87}Sr through the rivers to the sea water, resulting in the higher $^{87}Sr/^{86}Sr$ ratio, averaging 0.7119 globally (Palmer and Elderfield, 1985). The other is the hydrothermal system at mid-ocean ridges, which provides the predominantly non-radiogenic ^{86}Sr, resulting in the lower $^{87}Sr/^{86}Sr$ ratio, averaging 0.7035 globally (Palmer and Elderfield, 1985). The $^{87}Sr/^{86}Sr$ ratio of modern seawater is the result of the balance of Sr isotopes derived from these two sources, averaging 0.709073 ± 0.000003 (Denison et al., 1994). The major reasons leading to the higher $^{87}Sr/^{86}Sr$ ratio of the carbonates than that of the coeval seawater during the diagenetic process are as follows. 1) The formation water (or atmospheric fresh water) acquires radioactive ^{87}Sr by dissolution of the ^{87}Sr-rich siliciclastic sediments when flowing through them, and reacts with the carbonate minerals, leading to an increase in the marine $^{87}Sr/^{86}Sr$ ratio. 2) The deep formation water affected by silicate minerals provides radioactive ^{87}Sr to carbonate minerals, resulting in an increased $^{87}Sr/^{86}Sr$ ratio (Zhao and Wang, 2011). Based on the above analyses and the fact that the Qixia Formation dolomites have not been affected by atmospheric fresh water, the upward migration of deep hydrothermal fluids along faults through the underlying clastic rocks of the Qixia Formation results in the enrichment of ^{87}Sr and its consequent higher $^{87}Sr/^{86}Sr$ ratio than the coeval seawater in some dolomite samples.

6.6 Fluid Inclusions

The comparison shows that homogenization temperature of inclusions is the highest in D2, followed by D3, and is the lowest in D1. The salinity values of D2 and D3 are similar to each other, are higher than that of D1, and are generally 3–5 times higher than that of normal seawater. The salinity of normal seawater is 4.4% (Chen et al., 2012). Jiang et al. (2014) reported the largest buried depth of the Qixia Formation is 4,500 m and the corresponding paleotemperature is 116°C, after a study on the burial history in Well Kuang 2 drilled in the northwestern Sichuan Basin according to the Middle Permian paleo-geothermal gradient. As geomorphologically lower than Well Kuang 2, the Shuangyushi block to its southeast is speculated to have a lower paleotemperature than 116°C in the Qixia Formation. This is similar to the homogenization temperatures of inclusions in D1 and D3, which are lower than that in D2.

Chen et al. (2013) reported that the homogenization temperature of inclusions is 125°C–178°C in the southwestern Sichuan Basin. According to the research result of Jiang et al. (2014) reported that the homogenization temperature of inclusions is 120°C–195°C, and the salinity of 70 percent of inclusions exceeds 16%. Pei et al. (2021) reported that the homogenization temperature of primary inclusions in dolomites of the Middle Permian Qixia Formation, northwestern Sichuan Basin, ranges between 110°C and 120°C. It is concluded by this study that the salinity is 3–5 times higher than that of the coeval seawater, and the homogenization temperature of inclusions exceeds 100°C, which are similar to those measured in previous studies.

6.7 Saddle Dolomite (D2)

The results of thin section observations and SEM analysis show that the fractures and dissolution pores in the Qixia Formation are filled with saddle dolomite, asphalt, fluorite, apatite and other minerals. Gregg and Sibley (1984), Machel (1987) concluded that saddle dolomites are not the only indicator to identify hydrothermal dolomite, but are generally regarded as one of the key indicators of hydrothermal origin. Davies and Smith (2006) suggested that quartz, saddle dolomite, asphalt, fluorite and apatite are typical hydrothermal minerals. Huang et al. (2014) believed the saddle dolomites filling the geodes in the western Sichuan Basin are precipitated in the high-salinity and high-temperature fluid based on a study of carbon, oxygen isotopes and inclusion homogenization temperature. After an analysis of REE and inclusion homogenization temperature, Li et al. (2016) considered that the saddle dolomitization fluid is mainly derived from seawater or marine fluids in formation, and is affected by the thermal events related to the Emeishan large igneous province, but only to a limited degree. It is probably because the heat conduction effect overcame the dynamic barrier formed by of dolomite precipitation. Meng et al. (2017) identified that the saddle dolomites distinctly characterized by the more negative $\delta^{18}O$ values, which filled the geodes in the Qixia Formation in the northwestern Sichuan Basin, are the product of late hydrothermal fluid filling. Based on the study conducted by Pei et al. (2021) on the Qixia Formation dolomites in the northwestern Sichuan Basin, a large amount of hydrothermal minerals such as celestite, barite, fluorite, quartz and sphalerite have not been observed, with a small amount of saddle dolomites locally. It is considered that the Qixia Formation dolomites have been affected by small-scale hydrothermal solution, and hydrothermal dolomitization is not its major development mode. In this study, only a small amount of fluorite and saddle dolomites (D2) were observed in the Qixia Formation. The D2 is characterized with low $^{87}Sr/^{86}Sr$ ratio, high Fe and Mn contents, enrichment of light REE and depletion of heavy REE, weak-medium slightly negative anomaly of Eu and negative anomaly of Ce. Its $\delta^{13}C$ values are distributed within the variation range of normal seawater, and $\delta^{18}O$

values are more negative. It has higher $^{87}Sr/^{86}Sr$ ratio than the coeval seawater, and higher homogenization temperature of inclusions than D1. It is indicated that the saddle dolomitization fluid in the Qixia Formation is mainly derived from the seawater or marine fluids in formation, and is affected by high-temperature hydrothermal solution.

Moore (2001) concluded that a buried depth as small as 500 m allows the formation of stylolites in carbonates, especially for micro-stylolites, it could be smaller. When studying the medium-coarse crystalline dolomite of the Qixia Formation in the northwestern Sichuan Basin, Huang et al. (2013) and Meng et al. (2017) found that the stylolites of different stages cut across dolomite crystals, and the smallest formation depth of stylolites generally ranges from less than 600–1,000 m, inferring that the formation of medium-coarse crystalline should not be later than the shallow burial stage. It was proposed by Huang et al. (2013) in a study of the Qixia Formation hydrothermal dolomites in the western Sichuan Basin that the burial depth of the Qixia Formation was shallow less than 500 m, when the Emeishan basalt erupted. The rocks were not fully consolidated and had a high water/rock ratio, the increased temperature led to dolomitization through overcoming the dynamic barrier of dolomite precipitation, and the diagenetic fluid was still seawater. Li et al. (2020) inferred from the petrological and geochemical analyses that the Qixia Formation dolomites in the northwestern Sichuan Basin were formed early, and should have formed a certain scale in the sedimentary - pene-sedimentary period to the initial stage of shallow burial. From the homogenization temperature of inclusions and the single-well burial history of the Qixia Formation dolomites, Jiang et al. (2014) and Pei et al. (2021) concluded that the dolomites were probably formed earlier than the Middle-Late Triassic Period, with the reference to the paleo-geothermal gradient. The age of the Qixia Formation dolomites in the northwestern Sichuan Basin measured by Zeng et al. (2020) is 228–257 Ma using the U-Pb radioisotope dating method, and the formation time of crystalline dolomite was determined as the Middle-Late Triassic Period. Jicha et al. (2019), Wu et al. (2020) and Gregory et al. (2020) believed that the eruption time of the Emeishan basalt is 257–260 Ma. On the basis of the researches referred above as well as the petrological characteristics, the dolomitization process of the Qixia Formation was affected by the Emeishan basalt eruption, and the dolomites were formed in a shallow burial environment and not later than the Middle-Late Triassic Period.

In conclusion, the dolomitization fluids of the Qixia Formation in the Shuangyushi block, northwestern Sichuan Basin, are mainly derived by seawater or marine fluids sealed in pores under shallow-burial environment. The dolomites were alternated by deep high-salinity hydrothermal fluids in the late stage, and were formed before the Middle-Late Triassic Period, which could be explained by the superposition of burial dolomitization and hydrothermal dolomitization models.

7 CONCLUSION

1) The Qixia Formation in the Shuangyushi block, northwestern Sichuan Basin, is mainly deposited in the platform-margin shoal environment, and is dominated by highly crystallized dolomites. The dolomite crystals are mainly medium, coarse, medium-coarse and anisometric crystals, with cloudy centers and clear rims, and include subhedral-euhedral crystals with straight crystal face and anhedral crystal with non-straight crystal face. It is originated from bioclastic limestone. In the cathodoluminescence (CL) images, the dolomites exhibit dark purple luminescent in the centers and generally show bright orange red luminescent in the rims.

2) The Qixia Formation dolomite (D1) is relatively highly ordered. The CaO and MgO contents show a negative correlation with each other. They are characterized by high Mg^{2+}/Ca^{2+} ratio, high Fe, Mn, Na contents and low Sr content. The REE distribution pattern of dolomites (D1) is similar to that of calcites (C1), which is characterized by LREE enrichment, HREE depletion, obvious Eu positive anomalies, and slightly Ce negative anomalies. The $\delta^{13}C$ and $\delta^{18}O$ values are distributed within their variation ranges of the coeval seawater, and $^{87}Sr/^{86}Sr$ values are higher than those of the coeval seawater. The homogenization temperature of inclusions is close to the paleo-geothermal temperature, and the salinity is 3–5 times higher than that of normal seawater.

3) The dolomitization fluids of the Qixia Formation in the Shuangyushi block, northwestern Sichuan Basin, are mainly derived by seawater or marine fluids sealed in pores in shallow-burial environment. The dolomites experienced late alternation by deep high-salinity hydrothermal fluids, and were formed before the Middle-Late Triassic Period.

DATA AVAILABILITY STATEMENT

The original contributions presented in the study are included in the article/**Supplementary Material**, further inquiries can be directed to the corresponding authors.

AUTHOR CONTRIBUTIONS

WX and GZ: Conceptualization, field collection, methodology, formal analysis, investigation, writing manuscript; CW and LZ: review and editing manuscript; JT: field collection, laboratory investigation, preparing manuscript; CX: petrography investigation; XY: isotope analysis.

FUNDING

This research is financially supported by the National Natural Science Foundation of China (project 41972109).

SUPPLEMENTARY MATERIAL

The Supplementary Material for this article can be found online at: https://www.frontiersin.org/articles/10.3389/feart.2022.904932/full#supplementary-material

REFERENCES

Bau, M., and Dulski, P. (1996). Distribution of Yttrium and Rare-Earth Elements in the Penge and Kuruman Iron-Formations, Transvaal Supergroup, South Africa. *Precambrian Res.* 79 (1-2), 37–55. doi:10.1016/0301-9268(95)00087-9

Chen, X., Zhao, W. Z., Liu, Y. H., Zhou, H., and Jiang, Q. C. (2013). Characteristics and Exploration Strategy of the Middle Permian Hydrothermal Dolomite in Southwestern Sichuan Basin. *Acta Pet. Sin.* 34, 460–466. doi:10.1016/0301-9268(95)00087-9 (in Chinese with English abstract).

Chen, X., Zhao, W. Z., Zhang, L. P., Zhao, Z. Z., Liu, Y. H., and Zhang, B. M. (2012). Discovery and Exploration Significance of Structure-Controlled Hydrothermal Dolomites in the Middle Permian of the Central Sichuan Basin. *Acta Pet. Sin.* 33, 562–569. doi:10.7623/syxb201204004 (in Chinese with English abstract)

Chen, Z. X., Li, W., Wang, L. N., Lei, Y. L., Yang, G., and Zhang, B. J. (2019). Structural Geology and Favorable Exploration Prospect Belts in Northwestern Sichuan Basin, SW China. *Petroleum Explor. Dev.* 46, 397–408. (in Chinese with English abstract) doi:10.1016/s1876-3804(19)60022-4

Davies, G. R., and Smith, L. B. (2006). Structurally Controlled Hydrothermal Dolomite Reservoir Facies: An Overview. *Bulletin* 90, 1641–1690. doi:10.1306/05220605164

Denison, R. E., Koepnick, R. B., Burke, W. H., Hetherington, E. A., and Fletcher, A. (1994). Construction of the Mississippian, Pennsylvanian and Permian Seawater 87Sr86Sr Curve. *Chem. Geol.* 112, 145–167. doi:10.1016/0009-2541(94)90111-2

Gregg, J. M., and Sibley, D. F. (1984). Epigenetic Dolomitization and the Origin of Xenotopic Dolomite Texture. *J. Sediment. Petrology* 54, 908–931. doi:10.1306/212F8535-2B24-11D7-8648000102C1865D

Gromet, L. P., Haskin, L. A., Korotev, R. L., and Dymek, R. F. (1984). The "North American Shale Composite": Its Compilation, Major and Trace Element Characteristics. *Geochimica Cosmochimica Acta* 48, 2469–2482. doi:10.1016/0016-7037(84)90298-9

Han, Y. X., Li, Z., Han, D. L., Peng, S. T., and Liu, J. Q. (2009). REE Charaeteristics of Matrix Dolomites and its Origin of Lower Ordovician in Eastern Tabei Area, Tarim Basin. *Aeta Petrol. Sin.* 25, 2405–2416 (in Chinese with English abstract).

He, X. Y., Shou, J. F., Shen, A. J., Wu, X. N., Wang, Y. S., Hu, Y. Y., et al. (2014). Geochemical Characteristics and Origin of Dolomite: A Case Study from the Middle Assemblage of Majiagou Formation Member 5 of the West of Jingbian Gas Field, Ordos Basin, North China. *Petroleum Explor. Dev.* 41, 39–52. doi:10.1016/s1876-3804(14)60048-3 (in Chinese with English abstract)

He, Y., Liu, B., Liu, H. G., Shi, K. B., Wang, Y. C., and Jiang, W. M. (2018). Origin of Mg-Rich-Fluids and Dolomitization of Lower Ordovician Penglaiba Formation at Tongguzibulong Outcrop in the Northwestern Margin of Tarim Basin. *Acta Sci. Nat. Univ. Pekin.* 54, 781–791. (in Chinese with English abstract).

Hu, A. P., Pan, L. Y., Hao, Y., Shen, A. J., and Gu, M. F. (2018). Origin, Characteristics and Distribution of Dolostone Reservoir in Qixia Formation and Maokou Formation, Sichuan Basin, China. *Mar. Orig. Pet. Geol.* 23, 39–52. (in Chinese with English abstract).

Huang, S. J. (1997). A Study on Carbon and Strontium Isotopes of Late Paleozoic Carbonates in the Upper Yangtze Platform. *Acta Geol. Sin.* 71, 45–53. (in Chinese with English abstract).

Huang, S. J., Lan, Y. F., Huang, K. K., and Lv, J. (2014). Vug Fillings and Records of Hydrothermal Activity in the Middle Permian Qixia Formation, Western Sichuan Basin. *Acta Petrol. Sin.* 30, 687–698. doi:10.1134/S1075701514020044 (in Chinese with English abstract).

Huang, S. J., Li, X. N., Huang, K. K., Lan, Y. F., Lv, J., and Wang, C. M. (2012). Authigenic Noncarbonate Minerals in Hydrothermal Dolomite of Middle Permian Qixia Formation in the West of Sichuan Basin, China. *J. Chengdu Univ. Technol. Sci. Technol. Ed.* 39, 343–352. doi:10.3969/j.issn.1671-9727.2012.04.001 (in Chinese with English abstract).

Huang, S. J., Pan, X. Q., Lv, J., Qi, S. C., Huang, K. K., Lan, Y. F., et al. (2013). Hydrothermal Dolomitization and Subsequent Retrograde Dissolution in Qixia Formation , West Sichuan : A Case Study of Incomplete and Halfway- Back Dolomitization. *J. Chengdu Univ. Technol. Sci. Technol. Ed.)* 40, 288–300. doi:10.3969/j.issn.1671-9727.2013.03.09 (in Chinese with English abstract).

Huang, X. P., Yang, T. Q., and Zhang, H. M. (2004). Research on the Sedimentary Facies and Exploration Potential Areas of Lower Permian in Sichuan Basin. *Nat. Gas. Ind.* 24, 10–12. doi:10.3321/j.issn:1000-0976.2004.01.004 (in Chinese with English abstract).

Jiang, L., Cai, C., Worden, R. H., Crowley, S. F., Jia, L., Zhang, K., et al. (2016). Multiphase Dolomitization of Deeply Buried Cambrian Petroleum Reservoirs, Tarim Basin, North-West China. *Sedimentology* 63, 2130–2157. doi:10.1111/sed.12300

Jiang, Q. C., Hu, S. Y., Wang, Z. C., Wang, T. S., Li, Q. F., and Qu, X. F. (2014). Genesis of Medium-Macro-Crystalline Dolomite in the Middle Permian of Sichuan Basin. *Oil Gas Geol.* 35, 503–510. (in Chinese with English abstract).

Jiang, Z. B., Wang, Z. X., Zeng, D. M., Lu, T. M., Wang, B. Q., and Zhang, J. Y. (2009). Constructive Diagenesis and Porosity Evolution in the Lower Permian Qixia Formation of Northwest Si Chuan. *Geol. China* 36, 101–109. doi:10.3969/j.issn.1000-3657.2009.01.008 (in Chinese with English abstract).

Jicha, B. R., Singer, B. S., and Li, Y. (2019). Intercalibration of 40Ar/39Ar Laboratories in China, the USA and Russia for Emeishan Volcanism and the Guadalupian-Lopingian Boundary. *Natl. Sci. Rev.* 6, 614–616. doi:10.1093/nsr/nwz044

Jin, M. D., Tan, X. C., Li, B. S., Zhu, X., Zeng, W., and Lian, C. B. (2019). Genesis of Dolomite in the Sinian Dengying Formation in the Sichuan Basin. *Acta Sedimentol. Sin.* 37, 443–454. doi:10.14027/j.issn.1000-0550.2018.148 (in Chinese with English abstract)

Jin, Z. K., and Feng, Z. Z. (1999). Origin of Dolostones of the Lower Permian in East Yunnan-West Sichuan:Dolomitization through Leaching of Basalts. *Acta Sedimentol. Sin.*, 383–389. doi:10.14027/j.cnki.cjxb.1999.03.008 (in Chinese with English abstract).

Li, B., Wang, X. Z., Xie, S. Y., Feng, M. Y., Yang, X. F., Huo, F., et al. (2020). Characteristics and Genesis of the Middle Permian Qixia Formation Dolomite in the Northwestern Sichuan Basin. *Chin. J. Geol.* 55, 183–199. doi:10.12017/dzkx.2020.013 (in Chinese with English abstract)

Li, R. B., Duan, J. B., Pan, L., and Li, H. (2021). Genetic Mechanism and Main Controlling Factors of the Middle Permian Maokou Formation Dolomite Reservoirs in the Eastern Sichuan Basin. *Nat. Gas. Geosci.* 32, 1347–1357. doi:10.11764/j.issn.1672-1926.2021.04.014 (in Chinese with English abstract).

Li, X. N., Huang, S. J., Huang, K. K., Yuan, T., and Zhong, Y. J. (2016). Geochemical Characteristics of Middle Permian Qixia Fm Dolomitized Marine Fluids in the Sichuan Basin. *Nat. Gas. Ind.* 36, 35–45. doi:10.3787/j.issn.1000-0976.2016.10.00 (in Chinese with English abstract).

Liu, W. D., Zhong, D. K., Yi, H., Sun, H. T., Liang, X. Q., Li, R. R., et al. (2021). Development Characteristics and Main Controlling Factors of Ultra-deep Dolomite Reservoirs of the Qixia Formation in the Northwestern Sichuan Basin. *J. China Univ. Min. Technol.* 50, 342–362. doi:10.14027/j.issn.1000-0550.2020.050 (in Chinese with English abstract).

Machel, H.-G. (1987). Saddle Dolomite as a By-Product of Chemical Compaction and Thermochemical Sulfate Reduction. *Geol* 15, 936–940. doi:10.1-130/0091-7613(1987)152.0.CO

Meng, S., Zhou, J. G., Yang, L., Hao, Y., and Lou, X. (2017). Genesis of Medium-Coarse Crystalline Dolomite of Middle Permian Qixia Formation, Western Sichuan. *Mar. Orig. Pet. Geol.* 22, 75–83. doi:10.3969/j.issn.1672-9854.2017.01.010 (in Chinese with English abstract).

Michard, A., and Albarède, F. (1986). The REE Content of Some Hydrothermal Fluids. *Chem. Geol.* 55, 51–60. doi:10.1016/0009-2541(86)90127-0

Moore, C. H. (2001). *Carbonate Diagenesis and Porosity*. Amsterdam: Elsevier Science Publisher, 1–16.

Palmer, M. R., and Elderfield, H. (1985). Sr Isotope Composition of Sea Water over the Past 75 Myr. *Nature* 314, 526–528. doi:10.1038/314526a0

Pei, S. Q., Wang, X. Z., Li, R. R., Yang, X., Long, H. Y., Hu, X., et al. (2021). Burial Dolomitization of Marginal Platform Bank Facies and its Petroleum Geological Implications: The Genesis of Middle Permian Qixia Formation Dolostones in the Northwestern Sichuan Basin. *Nat. Gas. Ind.* 41, 22–29. doi:10.3787/j.issn.1000-0976.2021.04.003 (in Chinese with English abstract).

Ren, Y., Zhong, D. K., Gao, C. L., Yang, X. Q., Xie, R., Li, Z. P., et al. (2016). Geochemical Characteristics, Genesis and Hydrocarbon Significance of Dolomite in the Cambrian Longwangmiao Formation, Eastern Sichuan Basin. *Acta Pet. Sin.* 37, 1102–1115. doi:10.7623/syxb201609004 (in Chinese with English abstract).

Shellnutt, J. G., Pham, T. T., Denyszyn, S. W., Yeh, M.-W., and Tran, T.-A. (2020). Magmatic Duration of the Emeishan Large Igneous Province: Insight from Northern Vietnam. *Geology* 48, 457–461. doi:10.1130/G47076.1

Sun, H. T., Zhang, Y. Y., Liu, H. L., Xie, R., Yang, X. Q., and Ren, Y. (2018). Typological Analysis and Genetic Mechanism of Dolomite in the Lower Cambrian Longwangmiao Formation, Eastern Sichuan Basin. *Oil Gas Geol.* 39, 318–329. (in Chinese with English abstract).

Tian, J. C., Lin, X. B., Zhang, X., Peng, S. F., Yang, C. Y., Luo, S. B., et al. (2014). The Genetic Mechanism of Shoal Facies Dolomite and its Additive Effect of Permian Qixia Formation in Sichuan Basin. *Acta Petrol. Sin.* 30, 679–686. (in Chinese with English abstract).

Veizer, J., Ala, D., Azmy, K., Bruckschen, P., Buhl, D., Bruhn, F., et al. (1999). 87Sr/86Sr, δ13C and δ18O Evolution of Phanerozoic Seawater. *Chem. Geol.* 161, 59–88. doi:10.1180/minmag.1998.62A.3.16510.1016/s0009-2541(99)00081-9

Walker, G., Abumere, O. E., and Kamaluddin, B. (1989). Luminescence Spectroscopy of Mn2+rock-Forming Carbonates. *Mineral. Mag.* 53, 201–211. doi:10.1180/minmag.1989.053.370.07

Wang, D., Yuan, M., Duan, W. H., Xu, Z. B., and He, Y. B. (2011). The Dolostone of Qixia Formation in Middle Permian of Northwest Sichuan. *J. Oil Gas Technol.* 33, 46–49. doi:10.3969/j.issn.1000-9752.2011.06.010 (in Chinese with English abstract).

Wu, Q., Ramezani, J., Zhang, H., Yuan, D. X., Erwin, D. H., Henderson, C. M., et al. (2020). High-precision U-Pb Zircon Age Constraints on the Guadalupian in West Texas, USA. *Palaeogeogr. Palaeoclimatol. Palaeoecol.* 548, 1–14. doi:10.1016/j.palaeo.2020.10966810.1016/j.palaeo.2020.109668

Yang, Y., Gao, F. H., and Pu, X. G. (2014). REE Characteristics and Genesis of Dolostones from Paleogene Shahejie Formation in Qikou Depression. *J. China Univ. Petroleum* 38, 1–9. doi:10.3969/j.issn.1673-5005.2014.02.001 (in Chinese with English abstract).

Yang, Y. M., Chen, C., Wen, L., Chen, X., Liang, H., Liu, R., et al. (2018). Characteristics of Buried Structures in the Northern Longmenshan Mountains and its Significance to Oil and Gas Exploration in the Sichuan Basin. *Nat. Gas. Ind.* 38, 8–15. doi:10.3787/j.issn.1000-0976.2018.08.002 (in Chinese with English abstract).

Yang, Y. R., Zhang, Y., Xie, C., Chen, C., Zhang, X. L., Chen, S. L., et al. (2019). Hydrothermal Action of Middle Permian Qixia Formation in Northwestern Sichuan Basin and its Effect on Reservoirs. *Lithol. Reserv.* 31, 44–53. doi:10.12108/yxyqc.20190605 (in Chinese with English abstract).

Yi, H. S., Lin, J. H., Zhao, X. X., Zhou, K. K., Li, J. P., and Huang, H. G. (2008). Geochemistry of Rare Earth Elements and Origin of Positive Europium Anomaly in Miocene-Oligocene Lacustrine Carbonates from Tuotuohe Basin of Tibetan Plateau. *Acta Sedimentol. Sin.* 26, 1–10. doi:10.14027/j.cnki.cjxb.2008.01.002 (in Chinese with English abstract).

Zeng, X. Y., Zhong, D. K., Li, R. R., HuSun, X. H. T., Liu, W. D., Qin, P., et al. (2020). Genesis of Dolomites of the Lower Permian Qixia Formation in the Shuangyushi Area , Northwestern Sichuan Basin. *J. China Univ. Min. Technol.* 49, 974–990. doi:10.13247/j.cnki.jcumt.001179 (in Chinese with English abstract).

Zhang, Y. B. (1982). Dolomitization in Permian Rocks in Sichuan Basin. *Acta Pet. Sin.* 3, 29–33. doi:10.7623/syxb198201005 (in Chinese with English abstract).

Zhao, W. W., and Wang, B. Q. (2011). Geochemical Characteristics of Dolomite from 5th Member of the Ordovician Majiagou Formation in Sulige Area, Ordos Basin. *Acta Geosci. Sin.* 32, 681–690. doi:10.3975/cagsb.2011.06.05 (in Chinese with English abstract).

Zhong, Q. Q., Huang, S. J., Zhou, M. L., Tong, H. P., Huang, K. K., and Zhang, X. H. (2009). Controlling Factors of Order Degree of Dolomite in Carbonates:A Case Study from Lower Paleozoic in Tahe Oilfield and Triassic in Northeastern Sichuan Basin. *Lithol. Reserv.* 29, 50–55. doi:10.3969/j.issn.1673-8926.2009.03.010 (in Chinese with English abstract).

Zhu, C. Q., Xu, M., Yuan, Y. S., Zhao, Y. Q., Shan, J. N., He, Z. G., et al. (2010). Palaeo-geothermal Response and Record of the Effusing of Emeishan Basalts in Sichuan Basin. *Chin. Sci. Bull.* 55, 474–482. doi:10.1007/s11434-009-0490-y (in Chinese with English abstract)

Conflict of Interest: Authors GZ, JT, CX were employed by the PetroChina Southwest Oil and Gas Field Company. CW was employed by the Changqing Oilfield Company. LZ was employed by the Central Sichuan Gas Field of Southwest Oil and Gas Field Company.

The remaining authors declare that the research was conducted in the absence of any commercial or financial relationships that could be construed as a potential conflict of interest.

Publisher's Note: All claims expressed in this article are solely those of the authors and do not necessarily represent those of their affiliated organizations, or those of the publisher, the editors and the reviewers. Any product that may be evaluated in this article, or claim that may be made by its manufacturer, is not guaranteed or endorsed by the publisher.